Observation of Events with an Energetic Forward Neutron in Deep Inelastic Scattering at HERA

ZEUS Collaboration

Abstract

In deep inelastic neutral current scattering of positrons and protons at the center of mass energy of 300 GeV, we observe, with the ZEUS detector, events with a high energy neutron produced at very small scattering angles with respect to the proton direction. The events constitute a fixed fraction of the deep inelastic, neutral current event sample independent of Bjorken x and Q^2 in the range $3 \cdot 10^{-4} < x_{\mathrm{BJ}} < 6 \cdot 10^{-3}$ and $10 < Q^2 < 100$ GeV^2.

1   Introduction

The general features of the hadronic final state in deep inelastic lepton nucleon scattering (DIS) are well described by models inspired by Quantum Chromodynamics (QCD). In these models the struck quark and the colored proton remnant evolve into a system of partons which fragments into hadrons. Many of these models neglect peripheral processes, which are characterized by leading baryons.

A recent example of peripheral processes is the observation by ZEUS [1] and H1 [2] of DIS events with large rapidity gaps. These events are distinguished by the absence of color flow between the final state baryonic system and the fragments of the virtual photon, and they have been interpreted as arising from diffraction. In the language of Regge trajectories, a pomeron $\mathbb{P}$, with the quantum numbers of the vacuum, is exchanged between the proton and the virtual photon.

Another example is provided by meson exchange [3, 4, 5, 6, 7, 8], which plays a major role in peripheral hadronic scattering. In this process, the incoming proton fluctuates into a baryon and a meson. At HERA energies, the lifetime of this state can be sufficiently long that the lepton may interact with the meson. In $p \rightarrow p$ transitions the exchange of neutral mesons occurs together with diffractive scattering. These contributions may be separable by measuring the proton momentum distribution. On the other hand, $p \rightarrow n$ transitions signal events where charged meson exchange could dominate [9, 10], regardless of the neutron momentum. The pion, being the lightest meson, may provide the largest contribution to the cross section. Isolation of the one pion exchange contribution would provide the opportunity to study virtual gamma pion interactions and thereby determine the structure function of the pion.

In order to study these issues we have installed a hadronic calorimeter to detect high energy forward going neutrons produced in DIS ($ep \rightarrow en+$anything) at HERA. This paper reports the first observation of such events, showing clear evidence of sizeable leading neutron production.

2   Experimental setup

The data were collected with the ZEUS detector during 1994 while HERA collided 153 ep bunches of 27.5 GeV positrons and 820 GeV protons. In addition, 15 unpaired bunches of positrons and 17 unpaired bunches of protons circulated, permitting a measurement of beam associated backgrounds. The data sample used in this analysis corresponds to an integrated luminosity of 2.1 pb^{-1}.

The present analysis makes use of a test Forward Neutron Calorimeter (FNC II) [11] installed at the beginning of 1994 in the HERA tunnel at $\theta = 0$ degrees, $Z = 101$ m, downstream of the interaction point[1]. The layout of the beam line and calorimeter is shown schematically in Fig. 1. FNC II, located after the final station of the ZEUS Leading Proton Spectrometer (LPS), was an enlarged and improved version of the original test Forward

---

[1]The ZEUS coordinate system is defined as right handed with the Z axis pointing in the proton beam direction and the X axis horizontal, pointing towards the center of HERA.

Neutron Calorimeter (FNC I) which operated in 1993. The design, construction and calibration of FNC II was similar to FNC I [12, 13]. Both devices were iron-scintillator sandwich calorimeters read out with wavelength shifter light guides coupled to photomultiplier tubes (PMT). The unit cell consisted of 10 cm of iron followed by 0.5 cm of SCSN-38 scintillator. FNC II contained 17 unit cells comprising a total depth of 10 interaction lengths. It was 40 cm wide and 30 cm high, divided vertically into three 10 cm towers read out on both sides. There was no longitudinal subdivision in the readout.

The neutron calorimeter was situated downstream of the HERA dipoles which bend the 820 GeV proton beam upwards. Charged particles originating at the interaction point were swept away from FNC II. The aperture of the HERA magnets in front of FNC II limited the geometric acceptance as shown in Figs. 1(c) and (d). Between these magnets and FNC II the neutrons encountered inactive material, the thickness of which varied between one and two interaction lengths. Two scintillation veto counters preceded the calorimeter: one $30 \times 25 \times 5$ cm^3, and one $40 \times 30 \times 1$ cm^3. These counters were used offline to identify charged particles and thereby reject neutrons which interacted in the inactive material in front of FNC II. The calorimeter was followed by two scintillation counters, which were used in coincidence with the front counters to identify beam halo muons. The response of the counters to minimum ionizing particles was determined with these muons.

Energy deposits in FNC II were read out using a system identical to that of the ZEUS uranium scintillator calorimeter (CAL). In addition the rate of signals exceeding a threshold of 250 GeV was recorded. The accumulated counts provide the average counting rate of FNC II for each run.

The other components of ZEUS have been described elsewhere [14]. The CAL, the central tracking detectors (CTD,VXD), the small angle rear tracking detector (SRTD) which is a scintillator hodoscope in front of the rear calorimeter close to the beam pipe, and the luminosity monitor (LUMI) are the main components used for the analysis of DIS events [15].

3   Kinematics of deep inelastic events

In the present analysis the two particle inclusive reaction $ep \rightarrow en+$anything is compared with the single particle inclusive reaction $ep \rightarrow e+$anything. In both cases the scattered positron and part of the hadronic system, denoted by X, were detected in CAL. Energetic forward neutrons were detected in FNC II. The two particle inclusive events are specified by four independent kinematical variables: any two of x_{BJ}, Q^2, y, and W for the scattered lepton; and any two of x_{L}, p_{T}, and t for the leading baryon (see below).

Diagrams for one and two particle inclusive ep scattering are shown in Fig. 2(a) and (b). The conventional DIS kinematical variables describe the scattered positron: Q^2, the negative of the squared four–momentum transfer carried by the virtual photon γ^*,

$$Q^2 \equiv -q^2 = -(k - k')^2,$$

where k and k' are the four–momentum vectors of the initial and final state positron respectively; y, the energy transfer to the hadronic final state

$$y \equiv \frac{q \cdot P}{k \cdot P} \, ,$$

where P is the four–momentum vector of the incoming proton; x_{BJ}, the Bjorken variable

$$x_{\mathrm{BJ}} \equiv \frac{Q^2}{2q \cdot P} = \frac{Q^2}{ys} \,,$$

where s is the center-of-mass (c.m.) energy squared of the ep system; and W, the c.m. energy of the $\gamma^* p$ system,

$$W^2 \equiv (q + P)^2 = \frac{Q^2(1 - x_{\mathrm{BJ}})}{x_{\mathrm{BJ}}} + M_p{}^2,$$

where M_p is the mass of the proton.

The "double angle method" was used to determine x_{BJ} and Q^2 [16]. In this method, event variables are derived from the scattering angle of the positron and the scattering angle γ_H of the struck (massless) quark. The latter angle is determined from the hadronic energy flow measured in the main ZEUS detector,

$$\cos\gamma_H = \frac{(\sum_i p_X)^2 + (\sum_i p_Y)^2 - (\sum_i(E - p_Z))^2}{(\sum_i p_X)^2 + (\sum_i p_Y)^2 + (\sum_i(E - p_Z))^2} \,,$$

where the sums run over all CAL cells i, excluding those assigned to the scattered positron, and $\mathbf{p} = (p_X, p_Y, p_Z)$ is the momentum vector assigned to each cell of energy E. The cell angles are calculated from the geometric center of the cell and the vertex position of the event. Final state particles produced close to the direction of the proton beam give a negligible contribution to $\cos\gamma_H$, since these particles have $(E - p_Z) \simeq 0$.

In the double angle method, in order that the hadronic system be well measured, it is necessary to require a minimum hadronic energy in the CAL away from the beam pipe. A suitable quantity for this purpose is the hadronic estimator of the variable y, defined by

$$y_{\mathrm{JB}} \equiv \frac{\sum_i(E - p_Z)}{2E_e},$$

where E_e is the electron beam energy.

The two independent kinematical variables describing the neutron tagged by FNC II are taken to be its energy E_n and transverse momentum p_{T}. These quantities are related to the four-momentum transfer squared between the proton and the neutron, t, by

$$t \simeq -\frac{p_{\mathrm{T}}{}^2}{x_{\mathrm{L}}} - \frac{(1 - x_{\mathrm{L}})}{x_{\mathrm{L}}} \left(M_n^2 - x_{\mathrm{L}} M_p^2\right),$$

where M_n is the mass of the neutron and $x_{\mathrm{L}} \equiv E_n/E_p$, where E_p is the proton beam energy. The geometry of FNC II and the HERA beam line limited the angular acceptance of the scattered neutron to $\theta \lesssim 0.75$ mrad, and the threshold on energy deposits in FNC II restricted x_{L} to $x_{\mathrm{L}} > 0.3$.

The invariant mass of the hadronic system detected in the calorimeter, M_X, can be determined from the cell information in CAL; an approach similar to the double angle method is applied to calculate M_X. Given the energy, E_H, the momentum, p_H, and the polar angle, θ_H, of the hadronic system observed in the detector, the following formulae determine M_X: $\cos\theta_H = \sum_i p_Z / |\sum_i \mathbf{p}|$, where the sum runs over all calorimeter cells i, excluding those assigned to the positron, $p_H^2 = Q^2(1 - y)/\sin^2\theta_H$, $E_H = 2E_e y + p_H \cos\theta_H$, $M_X = \sqrt{E_H^2 - p_H^2}$.

The identification of neutral current deep inelastic events uses the quantity δ defined by

$$\delta \equiv \sum_i (E - p_Z) \ ,$$

where the sum runs over all CAL cells i. For fully contained neutral current DIS events, and neglecting CAL resolution effects and initial state radiation, $\delta = 2E_e$.

We also use the variable η_{max} which is defined as the pseudorapidity,

$$\eta \equiv -\ln \tan (\theta/2) \ ,$$

of the calorimeter cluster with energy greater than 400 MeV closest to the proton beam direction.

4   Monte Carlo simulation and studies

The response of FNC II was modeled by a Monte Carlo (MC) simulation using the GEANT program [17]. The model was inserted into the full simulation of the ZEUS detector and beam line. For neutrons incident on the face of the calorimeter the predicted energy resolution is approximately $\sigma(E_n) = 2.0\sqrt{E_n}$, with E_n in GeV. The predicted energy response of the calorimeter is linear to better than 5%.

To aid the study of energetic neutron production both in beam gas collisions and in DIS, a Monte Carlo generator was written for one pion exchange, which gives a cross section proportional to $|t| \cdot (1 - x_{\mathrm{L}})^{1 - 2\alpha_\pi(t)}/\alpha_\pi^2(t)$ (see, for example, [9]), where $\alpha_\pi(t) = \alpha'_\pi(t - m_\pi^2)$ is the pion trajectory and $\alpha'_\pi = 1$ GeV^{-2}. The code uses, as a framework, the HERWIG program [18]. Absorptive corrections to one pion exchange have been widely discussed (see, for example, [19, 20, 21]). To estimate such effects a simple prescription which replaces $|t|$ by $|t| + m_\pi^2$ in the numerator of the above expression was used. In addition to the one pion exchange model, the standard QCD inspired DIS models ARIADNE [22], HERWIG, and MEPS [23] were used to predict the forward neutron production.

To compare data with the expectations of all these models, the MC events produced by the generators were fed through the simulation of the ZEUS detector.

5   Calibration and acceptance of FNC II

The relative gains of the PMTs were determined by scanning each tower with a ^{60}Co gamma source using the procedure developed for the ZEUS CAL [24]. This was done at the end of the data taking period. Beam gas data taken in HERA were used for calibration. These data were obtained after the proton beam was accelerated to 820 GeV, but before positrons were injected. To reject events where the neutrons had showered in material upstream of FNC II, events were considered only when the energy deposited in the veto counters was below that of a minimum ionizing particle.

The HERA beam gas interactions occur at c.m. energies similar to those of $p \to n$ data measured at Fermilab and the ISR [25] where neutron spectra were found to be in good agreement with the predictions of one pion exchange [9, 25]. The energy scale of FNC II was determined by fitting the observed beam gas spectrum above 600 GeV to that expected from one pion exchange, folded with the response of FNC II as simulated by MC. The error in the energy scale is estimated as 5%.

Proton beam gas data taken during a special run at proton energies of 150, 300, 448, 560, 677, and 820 GeV showed that the energy response of FNC II was linear to within 4%.

To correct for the drift in gains of the PMTs, proton beam gas data were taken with an FNC trigger approximately every two weeks. The mean response of each tower showed variations between calibration runs at the level of 3%.

The overall acceptance for neutrons, $A_{\rm FNC}$, is independent of the acceptance of the main detector. To determine $A_{\rm FNC}$, the inactive material obscuring the aperture had to be modeled. About half of the inactive material was of simple geometric shape and included in the ZEUS detector simulation. The remainder, consisting mostly of iron between the beam line elements and FNC II, was modeled by an iron plate. The thickness of this plate was adjusted so that the resulting MC energy spectrum of neutrons from beam gas interactions matched the observed spectrum. Since the interaction of neutrons in the material leads, in general, to the loss of energy either by absorption and/or by particle emission outside the acceptance of FNC II, the observed energy spectrum is very sensitive to the amount of inactive material upstream. Therefore, in this study of inactive material, events in which the neutrons began showering upstream of FNC II were included in the spectrum; that is, no cut was made on charged particles in the scintillator counters in front of FNC II. The resulting thickness of the plate was 16±7 cm. Because of interactions in the inactive material, only about 15% of neutrons with energy $E_n > 250$ GeV which pass through the geometric aperture reach FNC II and survive the scintillator cuts. The acceptance is constant within 15% for neutrons with energy $400 < E_n < 820$ GeV scattered at a fixed angle in the range 0 to 0.7 mrad.

The overall acceptance assuming one pion exchange with the form described in Section 4 is $4.9^{+3.0}_{-1.9}\%$ for neutrons with $E_n > 400$ GeV and $|t| < 0.5$ GeV^2. The error quoted is dominated by the systematic error in estimating the amount of inactive material in front of FNC II.

To study the effect of uncertainties in the theoretical form of the cross section for one pion exchange, the part of the acceptance due to the geometric aperture, as shown in Fig. 1(d), was calculated for several proposed forms [7, 9, 10]. It was found to vary from approximately 32% to 35%. This part of the acceptance for ρ exchange varies between 10% and 30%, depending on the model [7, 26].

6   Triggering and data selection

The selection was almost identical to that used for the measurement of the structure function F_2 [15].

Events were filtered online by a three level trigger system [14]. At the first level DIS events were selected by requiring a minimum energy deposition in the electromagnetic section of the CAL. The threshold depended on the position in the CAL and varied between 3.4 and 4.8 GeV. For events selected with the analysis cuts listed below, this trigger was more than 99% efficient for positrons with energy greater than 7 GeV, as determined by Monte Carlo studies.

At the second level trigger (SLT), background was further reduced using the measured times of energy deposits and the summed energies from the calorimeter. The events were accepted if

$$\delta_{SLT} \equiv \sum_i E_i(1 - \cos\theta_i) > 24 \text{ GeV} - 2E_\gamma,$$

where E_i and θ_i are the energies and polar angles (with respect to the primary vertex position) of calorimeter cells, and E_γ is the energy deposit measured in the LUMI photon calorimeter. For perfect detector resolution and acceptance, δ_{SLT} is twice the positron beam energy (55 GeV) for DIS events, while for photoproduction events, where the scattered positron escapes down the beam pipe, δ_{SLT} peaks at much lower values.

The full event information was available at the third level trigger (TLT). Tighter timing cuts as well as algorithms to remove beam halo muons and cosmic muons were applied. The quantity δ_{TLT} was determined in the same manner as for δ_{SLT}. The events were required to have $\delta_{TLT} > 25$ GeV $- 2E_\gamma$. Finally, events were accepted as DIS candidates if a scattered positron candidate of energy greater than 4 GeV was found.

In the analysis of the resulting data set, further selection criteria were applied both to ensure accurate reconstruction of the kinematical variables, and to increase the purity of the sample by eliminating background from photoproduction. These cuts were:

$$E'_e > 8 \text{ GeV},$$
$$y_{\text{JB}} > 0.04, \ y_e < 0.95,$$
$$|X| > 14 \text{ cm or } |Y| > 13 \text{ cm},$$
$$-40 < Z_{\text{vertex}} < 40 \text{ cm},$$
$$35 < \delta < 65 \text{ GeV},$$

where y_e is y evaluated from the scattered positron energy, E'_e, and angle; X and Y are the impact position of the positron on the CAL as determined using the SRTD. The cut on $|X|, |Y|$ is a fiducial volume cut to avoid the region directly adjacent to the rear beam pipe.

Beam conditions sometimes resulted in a large FNC II counting rate from energy deposits above the threshold of 250 GeV. Runs were rejected if the counting rate, averaged over the run, was greater than 5 kHz in order to reduce the probability of a beam gas interaction randomly overlapping a true DIS event. Neutron tagged events were selected by requiring that FNC II show an energy deposit above threshold, and that the scintillation veto counters show an energy deposit below that of a minimum ionizing particle.

This study is restricted to events with $Q^2 > 10$ GeV^2 [1]. After these selections, 112k events remain containing 669 neutron tagged events constituting 0.6% of the sample.

7 Backgrounds

The counting rate of FNC II is predominantly due to protons interacting with residual gas in the beam pipe. As a result, the main background is due to the random overlap of energetic neutrons from beam gas interactions with genuine DIS events.

The fraction of beam gas triggers which survive the scintillation counter charged particle veto was measured to be 54±4%. The average raw counting rate of FNC II during the taking of ep data was 1.5 kHz leaving an effective counting rate of 833 Hz after the cuts. With 170 proton bunches in 220 HERA RF buckets and a crossing time of 96 ns, the overlap probability of a neutron with a random bunch was $1.0 \cdot 10^{-4}$. Since neutrons are tagged in 0.6% of the events,

$$\frac{\text{signal}}{\text{background}} = \frac{0.6 \cdot 10^{-2}}{1.0 \cdot 10^{-4}} = 60.$$

Thus only 1.7% of the neutron tagged events result from random overlaps. The same result is obtained if the background is calculated on a run by run basis.

The small random coincidence rate was confirmed by the rate of neutrons in non ep background events (cosmic rays and beam halo muons), and in a sample of random triggers.

For the DIS selection, the background from photoproduction was estimated to be less than 1% overall. A sample of photoproduction events was studied to rule out the possibility that the observed rate of neutrons in DIS was due to an anomalously large production rate of neutrons in photoproduction. A fractional rate in photoproduction comparable to that in DIS was found, verifying that the photoproduction background after the neutron tag was also less than 1%. The same conclusion holds for the background from beam gas interactions.

8   Characteristics of events with a leading neutron

The production of neutron tagged events with neutron energy $E_n > 400$ GeV was studied as a function of the lepton kinematical variables. Figure 2(c) shows a scatter plot of Q^2 versus x_{BJ} for a sample of 10k DIS events which were not required to have a neutron tag. All events in the full sample with a neutron tag are shown in Fig. 2(d). The neutron tagged events follow the distribution of DIS events. This is demonstrated quantitatively in Fig. 3(a) which shows the ratio r_{unc} of tagged events to all events, uncorrected for acceptance, as a function of x_{BJ}, Q^2 and W. Within the statistical accuracy, r_{unc} is consistent with being constant. This is also true if we take the ratio as a function of Q^2 in bins of x_{BJ} (not shown). Averaged over the x_{BJ} and Q^2 region the value of the ratio is $\overline{r}_{\mathrm{unc}} = 0.45 \pm 0.02 \pm 0.02$ % for $E_n > 400$ GeV. The first error is statistical and the second systematic. The latter is dominated by the neutron energy scale uncertainty.

Further insight is gained by examining the scatter plot of M_X versus W shown in Fig. 2(e) for the sample of 10k events. In this plot, there is a concentration of events at low M_X. These events are found to have a large rapidity gap (LRG), $\eta_{\mathrm{max}} < 2.0$. The neutron tagged events are distributed similarly to the full sample, as seen in Fig. 2(f). There is a concentration of a few events with a rapidity gap at low M_X, but most neutron tagged events are above the low M_X band.

The η_{max} distributions for all DIS events and for neutron tagged DIS events are similar in shape for $\eta_{\mathrm{max}} \gtrsim 2$ (Fig. 3(b)), showing an exponential rise for $2 \lesssim \eta_{\mathrm{max}} \lesssim 3.5$. Note that for $\eta_{\mathrm{max}} \gtrsim 4$ the distributions are strongly affected by limited acceptance towards the forward beam hole[2].

For $\eta_{\mathrm{max}} \lesssim 2.0$ there are relatively fewer neutron tags in the LRG events by a factor of about 2: the small η_{max} events represent 7% of all DIS events, but only 3% of the neutron tagged DIS events. This is shown in the plot of r_{unc} as a function of η_{max} in Fig. 3(c). LRG events with a leading neutron are expected, for instance, from diffractive production of a baryonic system decaying to an energetic forward neutron and from double peripheral processes, where a pomeron is exchanged between the virtual photon and the virtual pion emitted from the proton. This effect warrants further study.

The measured fraction of DIS events with a leading neutron with $E_n > 400$ GeV, $\overline{r}_{\mathrm{unc}} = 0.45 \pm 0.02 \pm 0.02$ %, can be compared with the predictions of models for DIS at HERA. ARIADNE [22], which is a colour dipole model including the boson gluon fusion process, in general gives a good description of the hadronic final state in DIS at HERA. The value of

---

[2]Values of $\eta_{\mathrm{max}} > 4.3$ are an artifact of the clustering algorithm, and may occur when particles are distributed in contiguous cells around the beam pipe.

$\overline{r}_{unc}$ predicted by ARIADNE is $0.13 \pm 0.05\%$, where the error is due to the uncertainty in the acceptance. This is a factor of about 3 less than that observed. Figure 4(a) shows the observed energy spectrum of neutrons tagged above 250 GeV by FNC II. The shape of the neutron energy distribution predicted by ARIADNE fails to describe the data, as seen from the dashed histogram in Fig. 4(a). The DIS models MEPS [23] and HERWIG [18] predict a higher rate of neutrons by about a factor of 2 but still fail to reproduce the observed energy spectrum.

The result of the one pion exchange Monte Carlo calculation of the expected spectrum is superimposed on the energy spectrum in Fig. 4(a), normalized to the total number of events above 400 GeV. There is reasonably good agreement between the Monte Carlo simulation and the data at energies above 400 GeV. At lower energies, other exchanges, such as the ρ, may become important. The neutron energy distribution shows no indication of varying with x_{BJ} or Q^2. This is demonstrated in Fig. 4(b) and (c) where the mean E_{AV} and width σ_E of the neutron energy distribution are shown as functions of x_{BJ} and Q^2.

If A_{FNC} as determined for one pion exchange is taken together with $\overline{r}_{unc}$ as measured in the data, $9.1^{+3.6}_{-5.7}\%$ of DIS events have a neutron with energy $E_n > 400$ GeV and $|t| < 0.5$ GeV^2. The prescription for absorptive corrections discussed in section 4 decreases this fraction by about 8%.

9   Conclusions

We have observed energetic forward neutron production in DIS at HERA. The neutrons are detected at very small scattering angles, $\theta \lesssim 0.75$ mrad, and at high $x_L \equiv E_n/E_p$, $x_L > 0.3$. Within present statistics leading neutron production is a constant fraction of DIS independent of x_{BJ} and Q^2 in the range $3 \cdot 10^{-4} < x_{BJ} < 6 \cdot 10^{-3}$ and $10 < Q^2 < 100$ GeV^2. Furthermore, the neutron energy spectrum shows no variation of its mean or width with x_{BJ} and Q^2. Neutrons with energy $E_n > 400$ GeV and $|t| < 0.5$ GeV^2 account for a substantial fraction (at the level of 10%) of DIS events.

Acknowledgments

References

[1] ZEUS Collab., M. Derrick et al., Phys. Lett. **B315** (1993) 481; ZEUS Collab., M. Derrick et al., Phys. Lett. **B332** (1994) 228.

[2] H1 Collab., T. Ahmed et al., Nucl. Phys. **B429** (1994) 477.

[3] J. D. Sullivan, Phys. Rev. **D5** (1971) 1732.

[4] V. R. Zoller, Z. Phys. **C53** (1992) 443.

[5] G. Levman and K. Furutani, DESY Report 95-142 (1995).

[6] W. Koepf, L. L. Frankfurt, and M. Strikman, Phys. Rev. **D53** (1996) 2586.

[7] B. Kopeliovich, B. Povh, and I. Potashinikova, hep-ph/9601291 and DESY Report 95-11 (1996).

[8] M. Przybycień, A. Szczurek, and G. Ingelman, DESY Report 96-073 (1996).

[9] M. Bishari, Phys. Lett. **B38** (1972) 510; J. Pumplin, Phys. Rev. **D8** (1973) 2249.

[10] H. Holtmann et al., Phys. Lett. **B 338** (1994) 363.

[11] ZEUS Collab., DESY PRC 93-08.

[12] S. Bhadra et al., Nucl. Instr. and Meth. **A354** (1995) 479.

[13] M. Brkić, Ph. D. thesis, University of Toronto, DESY F35D-95-10 (1995).

[14] ZEUS Collab., The ZEUS Detector Status Report (DESY 1993).

[15] ZEUS Collab., M. Derrick et al., DESY Report 96-076 (1996), to be submitted to Z. Phys.

[16] S. Bentvelsen, J Engelen, and P. Kooijman, Proceedings of the 1991 Workshop on Physics at HERA (DESY 1992) 23.

[17] R. Brun et al., CERN DD/EE/84-1 (1987).

[18] G. Marchesini et al., Comput. Phys. Commun. **67** (1992) 465.

[19] P. K. Williams, Phys. Rev. **181** (1969) 1963.

[20] E. Gotsman and U. Maor, Nucl. Phys. **B57** (1973) 575.

[21] F. Schrempp and B. Schrempp, Proceedings of the EPS International Conference (International Physics Series, Editrice Compositori, Bologna 1975) 682.

[22] L. Lönnblad, Comput. Phys. Commun. **71** (1992) 15; B. Andersson et al., Phys. Rep. **97** (1983) 31.

[23] G. Ingelman, Proceedings of the 1991 Workshop on Physics at HERA (DESY 1992) 1366; M. Bengtsson, G. Ingelman and T. Sjöstrand, Nucl. Phys. **B301** (1988) 554.

[24] U. Behrens et al., Nucl. Instr. and Meth. **A323** (1992) 611.

[25] J. Engler et al., Nucl. Phys. **B84** (1975) 70; J. Hanlon et al., Phys. Rev. Lett. **37** (1976) 967; G. Hartner, Ph. D. thesis, McGill University (1977), unpublished; B. Robinson et al., Phys. Rev. Lett. **34** (1975) 1475.

[26] H. Holtmann, A. Szczurek, and J. Speth, Nucl. Phys. **A569** (1996) 631; A. Szczurek, private communication.

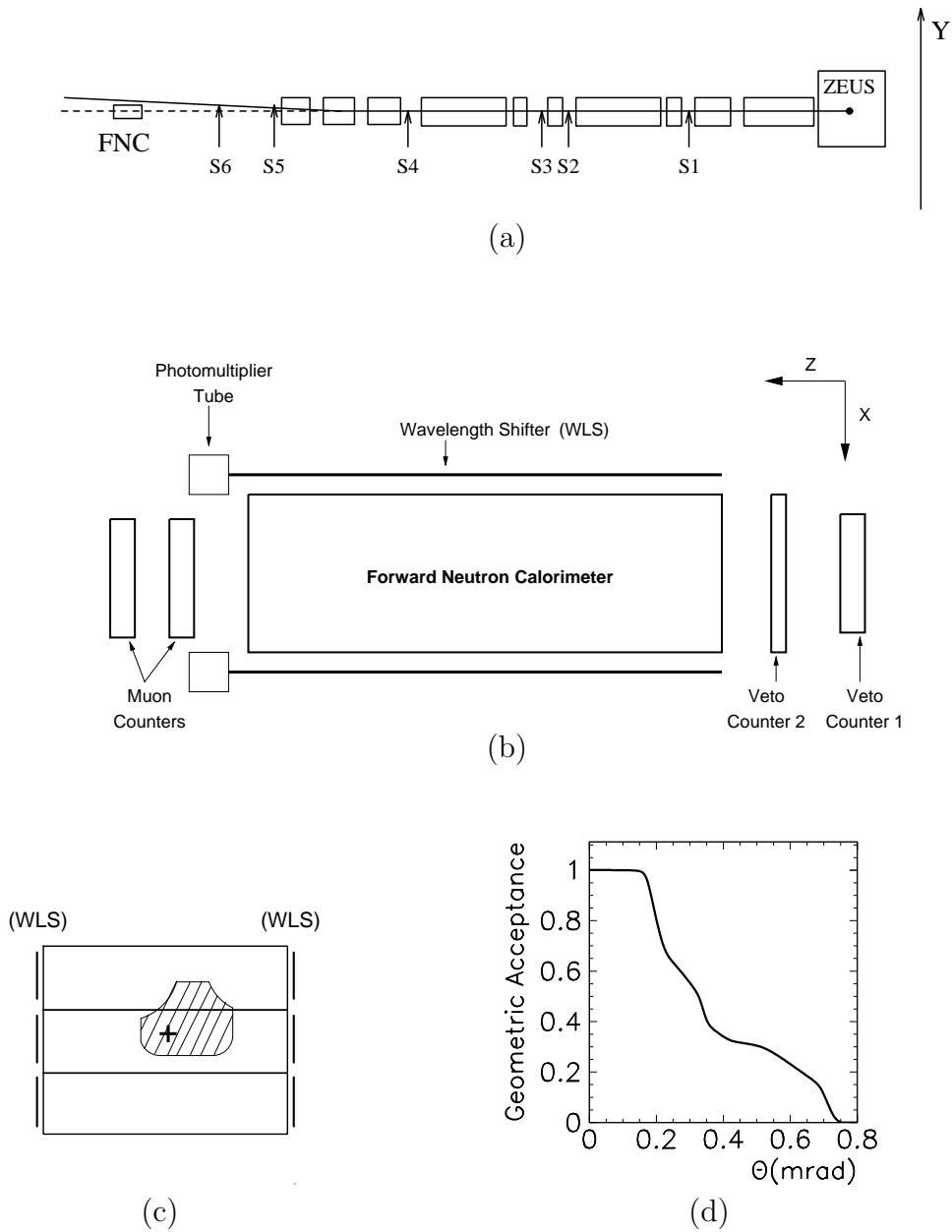[27] W. H. Smith et al., Nucl. Instr. and Meth. **A355** (1995) 278.

Figure 1: (a) Schematic layout of the proton beam line viewed from the side with FNC II (at $Z = 101$ m) below the beam pipe and downstream of LPS stations S1-S6. (b) Schematic drawing of FNC II viewed from the top. (c) Front view of FNC II showing the segmentation into three towers, and the projected region of geometric aperture allowed by the HERA magnets. The cross indicates the position of the zero degree line. (d) The geometric acceptance as a function of polar angle (scattering angle), integrated over azimuth.
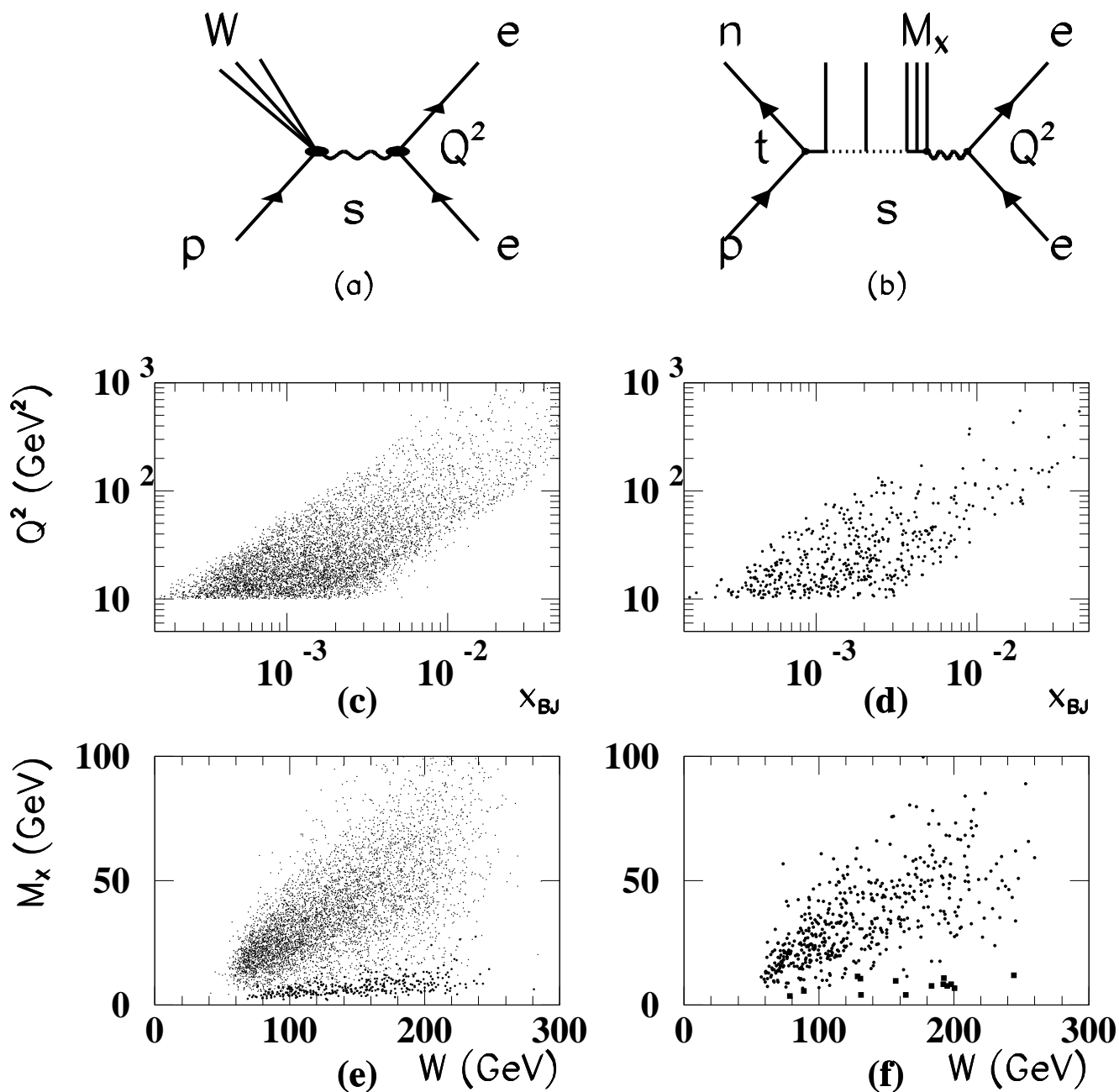
ZEUS 1994

Figure 2: (a) Diagram for the inclusive reaction $ep \to e$+anything, (b) for the two particle inclusive reaction $ep \to en$+anything, a special case of (a) where the hadronic system of mass W contains a forward neutron. The part of the hadronic system detected by CAL is denoted by X and has a mass M_X. (c) A scatter plot of Q^2 versus x_{BJ} for DIS events, and (d) neutron tagged DIS events with $E_n > 400$ GeV corresponding to (c). (e) A scatter plot of M_X versus W for DIS events. The events in the band at low M_X (larger dots) are the large rapidity gap events. (f) A scatter plot of M_X versus W for neutron tagged DIS events with $E_n > 400$ GeV. The LRG events are plotted as squares.
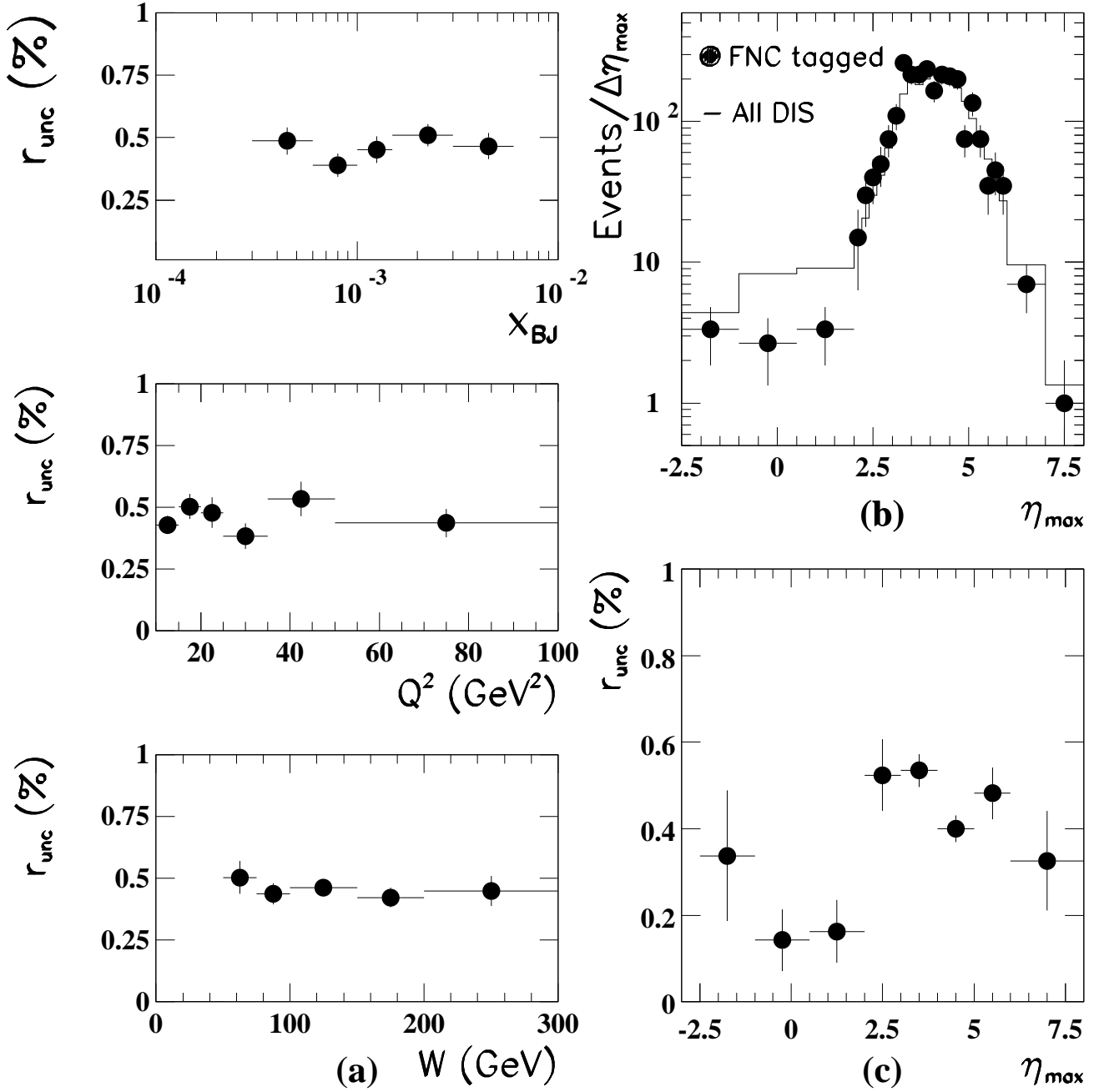
Figure 3: (a) The observed ratio of neutron tagged DIS events with $E_n > 400$ GeV to all DIS events as a function of x_{BJ}, Q^2, and W. (b) The data points show the η_{max} distribution for tagged DIS events with $E_n > 400$ GeV. The distribution for all DIS events multiplied by $0.45 \cdot 10^{-2}$ is superimposed as a histogram. (c) The observed ratio of tagged DIS events with $E_n > 400$ GeV to all DIS events as a function of η_{max}.
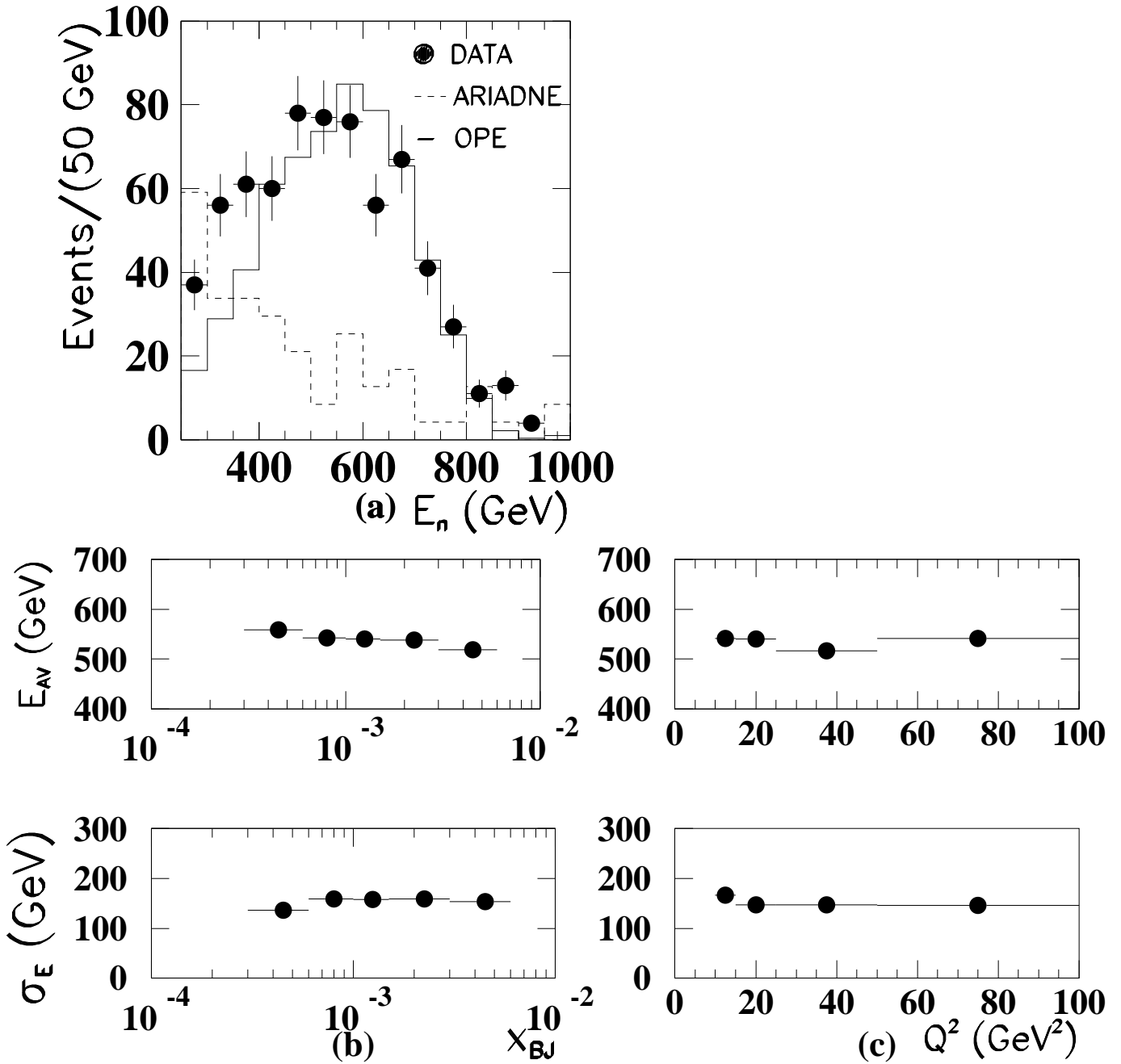
ZEUS 1994

Figure 4: (a) The energy distribution of neutrons tagged by FNC II, uncorrected for acceptance. The solid points are data and the histogram is the result of a one pion exchange DIS Monte Carlo calculation normalized to the number of events greater than 400 GeV. The dashed histogram gives the prediction of ARIADNE normalized to the same luminosity as the data. (b) and (c) The variation of the mean E_{AV} and width σ_E of the neutron energy spectrum above 250 GeV as a function of x_{BJ} and Q^2.